Far-Field Optical Microscopy of Single Metal Nanoparticles

MEINDERT A. VAN DIJK,
MARKUS LIPPITZ, AND MICHEL ORRIT*
MoNOS, Huygens Laboratory, Universiteit Leiden, P.O. Box 9504, 2300 RA Leiden, The Netherlands

Received January 24, 2005

ABSTRACT
Individual noble-metal particles, with sizes ranging from a few tenths to some hundreds of nanometers, can now be detected by far-field optics. Single-particle microscopy gives access to inhomogeneity, distributions, and fluctuations, which were previously hidden in ensemble experiments. Scattering methods rely on dark-field illumination, spectral signatures of the metal particles, or both. More advanced techniques provide high sensitivity and improved selectivity with respect to other scatterers by isolating metal-specific signals, for example the refractive index change due to heating of the environment by a pump beam or the time-resolved optical response of the particle to a short pump pulse. We review and compare linear and nonlinear methods in far-field optical microscopy that have reached the single-particle regime by means of scattered light, thermal effects, photoluminescence, or nonlinear frequency generation.

1. Motivation and Scope

Metal nanoparticles, with diameters ranging from a few tenths to some hundreds of nanometers, are natural bridges between molecules and extended solids. They are complex many-electron systems, where reduced sizes and quantum confinement of electrons and phonons give birth to fascinating new effects, potentially tunable with particle size and shape. Until a few years ago, the optical properties of metal particles were invariably studied on large ensembles. Recent progress and interest in optical microscopy have stimulated studies of *single* metal particles. In these experiments, particles are not only isolated from one another (i.e., they do not interact) but separated by distances so large that at most one particle is present in any given laser spot (the spot, a few hundreds of nanometers in diameter, is empty most of the time). Just as in the case of molecules[1,2] or semiconductor nanocrystals,[3] investigations of single metal particles add novel insight to conventional ensemble measurements by exploiting the following advantages:

• Inhomogeneity is suppressed. Even the best preparation methods yield populations of nanoparticles that differ not only in size and shape but also in the presence and distribution of bulk and surface defects, in chemical composition, etc. As in the case of semiconductor nanocrystals, of conjugated polymers, or of biomolecules, the selection of individuals is the only possible access to well-defined objects. This is a marked difference with chemically synthesized small molecules, the inhomogeneity of which usually exclusively arises from their local environment.

• Time-dependent fluctuations directly appear without any need for synchronization. Conventional ensemble methods rely on averages over many molecules. Therefore, they are completely blind to fluctuations whenever synchronization is not possible.

• Being small objects, single nanoparticles act as relays between a particular nanometer-sized spot and the macroscopic laboratory world. They can probe local properties or tag other mobile nano-objects such as biomolecules. In such applications, their main advantage with respect to fluorescent labels will be their stability and their low reactivity. Whereas dyes and semiconductor particles blink and eventually bleach under heavy laser illumination, the many electrons of a metal particle never stop interacting with light.

In this Account, we survey far-field optical studies of noble metal particles (mainly silver and gold) accessible to standard optical microscopes. Near-field optics have the additional advantages of higher spatial resolution and of correlations with topography,[4,5] but they are harder to implement and are largely limited to surfaces and interfaces (for a review, see ref 6). Since we are mainly interested by the particles themselves or by their uses as labels, we shall dwell on their "intrinsic" properties, those that arise from the "bulk" of the particle rather than from some localized electron states at its surface or vicinity. Such optically active states may arise at protrusions or from few-atom clusters or organic molecules adsorbed or bound at the surface of the particle. They may give rise to surface-enhanced Raman scattering (SERS), which has recently reached the single-molecule regime.[7] Although interesting in their own right and potentially useful for labeling, these local electron states widely fluctuate in number and nature from particle to particle. Moreover, they are prone to blinking and bleaching, as molecules and other few-electron systems are.

The Account is organized as follows. Part 2 summarizes electronic and optical properties of small metal particles relevant to far-field experiments. We then describe a number of methods for optical and spectroscopic study with increasing complexity. Scattering (part 3) arises whenever a small object presents a refractive index

Meindert A. van Dijk was born in 1979. He studied physics at the Vrije Universiteit in Amsterdam, where he graduated in 2003. Since then he has worked as a Ph.D. student in the group of Michel Orrit in Leiden. His current research interest is the time-resolved study of single nanoparticles.

Markus Lippitz was born in 1972, studied physics in Marburg and Milan, and received his Ph.D. from the University of Mainz in 2002. Since then he has been a Marie-Curie fellow in the group of Michel Orrit. His main research interest is in nonlinear optics with single molecules and single metal nanoparticles.

Born 1956 in Toulouse, France, Michel Orrit studied physics at E.N.S. in Paris. He worked at Bordeaux University and M.P.I. Göttingen on the spectroscopy of molecular excitons and Langmuir−Blodgett films. He started cryogenic fluorescence experiments on single molecules in 1990. He joined Leiden University in 2001 and is currently interested in the optical detection and microscopy of single nano-objects.

* To whom correspondence should be addressed. E-mail: orrit@molphys.leidenuniv.nl. Website: http://www.monos.leidenuniv.nl/.

10.1021/ar0401303 CCC: $30.25
Published on Web 04/06/2005

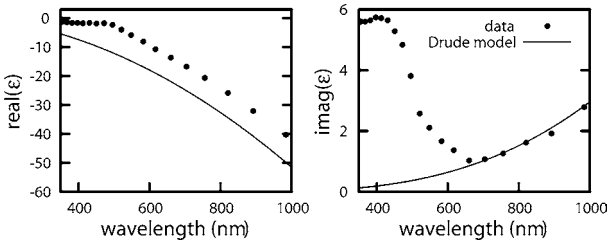

FIGURE 1. Dielectric function of gold[8] compared with the free electron model of Drude. The deviations are due to the interband contribution.

contrast with its surroundings. It can be easily visualized using dark-field illumination but quickly decreases with size. Because scattering from a metal particle is difficult to distinguish from that of other structures (e.g., cell organelles), various methods have been proposed to enhance selectivity. An important special case is scattering in the forward direction, which gives rise to extinction of the incident wave. Other waves can be made to interfere with the scattered wave, thus enhancing its visibility. A fundamentally different way to enhance the imaging contrast of the particles is to detect specific light-induced changes (part 4), which will be used as signatures of the metal particle. Examples are the heat produced by the motion of mobile electrons at a wavelength that only a metal can absorb or the short-lived changes of optical properties following absorption of a short laser pulse. Luminescence of metal structures (part 5) often arises from defects but possibly also from the bulk of very small particles. Finally, recently developed nonlinear imaging methods can be combined with the detection of nonlinear signals from single nanoparticles (part 6). We will briefly report recent experiments on the generation of third harmonic and conclude with an outlook for future research.

2. Linear Optical Properties

The optical properties of metals are, to a large extent, determined by conduction electrons. The response of these free electrons follows the Drude model. They collectively react to perturbation by an external electric field. The Coulomb restoring force between the electrons and the lattice leads to harmonic oscillations with the plasma frequency $\omega_p^2 = Ne^2/(m_e\epsilon_0)$ where N is the electron density and m_e the electron mass. The damping of the oscillation is described by a phenomenological damping constant, γ. In this model, the dielectric function, $\epsilon(\omega)$, equals

$$\epsilon(\omega) = 1 - \frac{{\omega_p}^2}{\omega(\omega + i\gamma)} \tag{1}$$

For noble metals, the contribution of the bound d-electrons to the optical properties cannot be neglected.[9] Visible to ultraviolet light also excites them to the conduction band, giving rise to interband transitions in the spectra. Figure 1 compares the measured dielectric function of gold[8] to the Drude model of free electrons.

The large negative value of the real part of the dielectric constant ϵ leads to a pronounced dielectric contrast between particle and surroundings, causing scattering.[10,11] Scattering produces new components of the electric field, $\mathbf{E}_{sca}$, that are related to the incoming field by the amplitude scattering matrix $\mathbf{X}$: $\mathbf{E}_{sca} \propto \mathbf{X}\,\mathbf{E}_{in}$. The scattering cross-section, σ_{sca}, is calculated by integrating the scattered power over a sphere in the far-field of the particle and dividing by the incident intensity. In the same way, the absorption cross-section, σ_{abs}, is calculated as the net energy flow into the far-field sphere divided by the intensity. The extinction cross-section, σ_{ext}, is the sum of both: $\sigma_{ext} = \sigma_{abs} + \sigma_{sca}$. The optical theorem relates σ_{ext} to the forward-scattering component of the scattering matrix $\mathbf{X}$ only, that is, it describes extinction as a destructive interference between incident and scattered waves. For a more detailed discussion, see textbooks.[10,11]

Mie's theory gives a multipolar series expansion of the extinction and scattering cross-section for spherical particles with a diameter d. The coefficients for the electric and magnetic multipoles involve Bessel-functions of the reduced size $x = \pi d n_{medium}/\lambda$ and the relative index of refraction $m = n_{sphere}/n_{medium}$. In a power series of x, the leading term is proportional to x^3 and appears in the electric dipole coefficient. Neglecting all higher orders of x gives the Rayleigh limit:

$$\sigma_{ext} = 2\frac{2\pi}{k^2}x^3\,\mathrm{Im}\left(\frac{m^2-1}{m^2+2}\right) \tag{2}$$

$$\sigma_{sca} = \frac{4}{3}\frac{2\pi}{k^2}x^6\left|\frac{m^2-1}{m^2+2}\right|^2 \tag{3}$$

This result can also be obtained by electrostatic calculations of the polarization of a small sphere, treating the sphere as an ideal dipole.[10] The scattering cross-section scales with the sixth power of the particle size, whereas the extinction scales with the third power only. Both the scattering and the absorption cross-section resonate at the frequency of the surface plasmon, determined by[9]

$$m^2 = \frac{\epsilon_{metal}}{\epsilon_{medium}} = -2 \tag{4}$$

Surface plasmons are localized oscillations of the electron density at a metal−dielectric interface.[12] Equation 4 shows that the plasmon resonance shifts when the surrounding medium changes, which is used for probing applications.[13,14]

Figure 2 shows extinction and absorption spectra for gold spheres in water, as calculated by Mie's theory. The larger the particle, the more important scattering becomes (Figure 2, top). Furthermore, a larger particle cannot be described as a point dipole. Retardation has to be taken into account by including higher orders of x in the derivation of eqs 2 and 3. This leads to a red-shift of the plasmon resonance with particle size,[9] as shown in Figure 2, bottom.

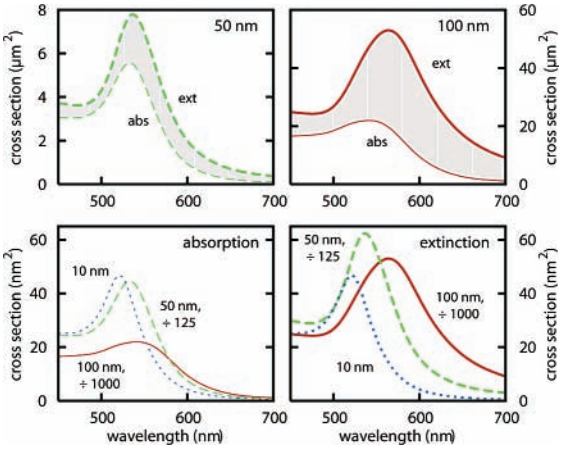

FIGURE 2. Extinction (thick lines) and absorption (thin lines) spectra of gold particles with a diameter of 10 nm (blue, dotted), 50 nm (green, dashed), and 100 nm (red, solid) plotted in different combinations of the same curves. The surrounding medium is water ($n = 1.3$). In the top panels, with increasing colloid size the additional scattering contribution to the extinction becomes more important; the gap between absorption and scattering spectra gets larger. In the bottom panels to compare colloids of different sizes the spectra are scaled with d^3 to the 10-nm particle. Both absorption and scattering spectra show a red shift and broadening of the plasmon resonance with particle size.

3. Scattering and Transmission Methods

Scattered light can be detected forward, backward, or laterally (with respect to the incoming beam). Experiments have covered all these possibilities. Placing the detector sideways to the scattering particle has the advantage that no excitation light reaches it. The particle appears on a black background. Dark-field illumination is a standard technique of biological microscopy that uses this effect. In the illuminating condenser lens, the inner part of the focused light cone is blocked and only the outer annular part is used. The detecting objective images only through the inner part of the cone. If no scatterer is present, no light can pass through the condenser−sample−objective combination. Schultz et al.[15] demonstrated that single silver particles with diameters between 40 and 100 nm can be distinguished from organelles in cells. The spectrum of the scattered light is well described by Mie's theory[16] and, for single particles, the absence of inhomogeneous broadening allows the quantification dephasing rate.[17] As discussed above, the plasmon resonance depends on the particle size and on the refractive index of the surrounding medium. Different sizes can thus be distinguished by the color of the scattered light (Figure 3), and individual particles can be used as sensors for their local environments.[13,14] The local environment is also modified by the presence of a second particle, leading to near-field interactions between metal particles.[18] For a review of particle plasmon resonances in biophysical applications, see Haes et al.[19] and Schultz.[20] White-light pulses combined with pump pulses give time-dependent scattering spectra of single colloids as demonstrated by Itoh et al.[21]

Illumination with evanescent waves is another technique that prevents the excitation light from reaching the detector. The excitation light falls under grazing incidence from the glass side on the glass−air interface and is totally reflected. Without scattering, no light would be detected in the far-field, but a scatterer converts the evanescent modes into propagating ones. Sönnichsen et al.[22] used this technique to investigate the plasmon damping of 70 nm wide gold islands that were prepared by electron-beam lithography. Nakayama et al.[23] followed the movement of gold-labeled actin filaments on myosin motor proteins.

In contrast to the experiments discussed above, Lindfors et al.[24] use the *backward* scattered light. The gold particles are prepared on a glass-immersion oil interface, which presents a small index step only. Therefore the intensities reflected by the interface and scattered by the particle are comparable. The total detected intensity, I_{det}, equals[24]

$$I_{det} = I_{in}(r^2 + |s|^2 - 2r|s| \sin \phi) \qquad (5)$$

where r is the (real) reflectivity constant of the interface and $s = |s| \exp(i\phi)$ is the relevant element of the amplitude scattering matrix **X**. The r^2 term gives a constant background. For larger particles, the scattered term, $|s|^2$, dominates, because it scales with d^6. For small particles, the cross-term dominates, leading to a reversal in the sign of the signal. Both effects are shown in Figure 4. While scattering leads to a strong signal for particles larger than about 40 nm, the cross-term still gives a signal for particles with a diameter of 10 nm and below.

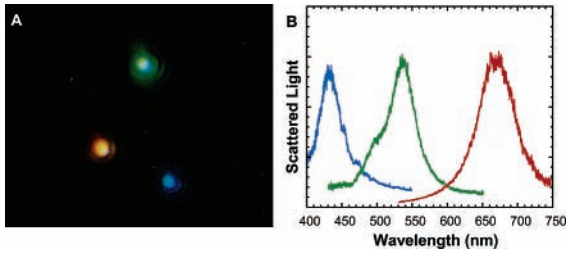

FIGURE 3. Dark-field image of silver particles of different sizes leading to different colors in the scattered white light.[15] The spot size is about 400 nm, and the height of the image is about 9 μm. The corresponding spectra are shown in the right panel. Reprinted with permission from ref 15. Copyright 2000 National Academy of Sciences, U.S.A.

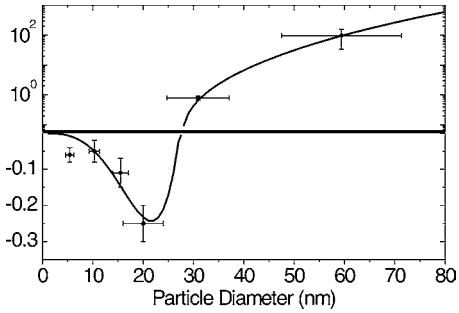

FIGURE 4. Size dependence of the detected signal (y-axis) for the interferometric detection scheme used by Lindfors et al.[24] Note the logarithmic scale for positive and the linear scale for negative values. Reprinted with permission from ref 24. Copyright 2004 American Physical Society.

When a 5-nm gold particle is moved in and out of the focus of the objective, the transmitted light intensity varies by about 10^{-5}. Already in 1986, such small gold particles could be visualized in a transmitted light video microscope by selectively stretching the contrast over a narrow intensity range combined with digital averaging over several seconds.[25] Arbouet et al.[26] detect the scattering and absorption of small particles in the transmitted light beam by lock-in amplification. Careful calibration of the detection path allowed them to measure the absolute value of the absorption cross-section.

4. Detection of Absorption-Induced Changes

According to the optical theorem, absorption and scattering are two sides of the same coin. The experiments discussed above use absorption and scattering to detect changes in the far-field light intensity. But absorption deposits energy in the particle. In the following section, we discuss two methods that detect the effect of this absorbed energy. One of them uses the photothermal effect to image nanoparticles,[27−29] and the other one is an interferometric pump−probe experiment that we recently developed.[30]

When light is absorbed by a metal particle, some of its energy is converted into heat, and the particle gets warmer. Heat diffuses out of the particle and changes the temperature of the surrounding medium. Because the index of refraction of the medium weakly depends on temperature ($dn/dT \approx 10^{-4}$ K^{-1} for water[27]), the phase of a transmitted light beam will be slightly shifted. This phase shift is measured in the photothermal imaging technique by a combination of differential interference contrast (DIC) and lock-in detection.[27,28]

A green (514 nm) heating laser is amplitude-modulated and focused on the sample, leading to damped heat waves around an absorbing particle. A red probe laser beam is split into two orthogonal polarized beams by a Wollaston prism that produces two diffraction-limited spots on the sample. One of these spots coincides with the green heating spot. Both parts of the probe beam are either reflected back by the sample−air interface[27] or recollimated with a second objective and reflected by an external mirror.[28] Both beams are recombined by a second pass through the Wollaston prism. If they have acquired a relative phase difference the resulting combined beam has an additional orthogonal polarization component that is detected by a photodiode and lock-in amplifier.

Boyer et al.[27] use this technique to image gold particles with a diameter of 5 nm at a signal-to-noise-ratio of about 10 (Figure 5). The analysis of the spot height distribution demonstrates that the spots stem from individual particles (otherwise, a progression of peaks would be expected in the histogram). The absorbed power leads to a temperature increase of about 15 K at the surface of the particle, dropping to about 3 K at a distance of 13 nm from the particle center. The experiment is sensitive only to the absorption of light. Scattering by large latex spheres[27] or organelles in cells[28] does not influence the signal.

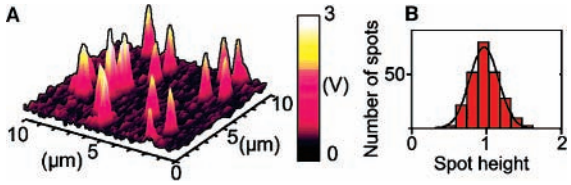

FIGURE 5. Photothermal image (A) of 5-nm gold particles on a glass substrate[27] showing a high signal-to-noise ratio and almost equal peak heights and histogram (B) of peak heights of about 200 spots. The narrow and monomodal distribution confirms that the spots correspond to single objects. Reprinted with permission from ref 27. Copyright 2002 American Association for the Advancement of Science.

In a recent experiment, Berciaud et al.[29] modified the experiment above, thus improving the sensitivity by 2 orders of magnitude. They detect the beating signal on the interference between the transmitted light of a probe beam and the light scattered by a particle, which is heated by an intensity-modulated pump beam. With this relatively simple technique, they were able to detect gold clusters of 1.4 nm diameter with a signal-to-noise-ratio of 10, while heating the clusters by only a few kelvin.

We propose an interferometric pump−probe experiment[30] to measure the optical properties of single metal particles on much shorter time scales.[31] When light is absorbed by a metal, electrons are excited to higher energy states. Within about 10 fs electron−electron scattering leads to a hot, thermalized electron gas. The electrons then scatter with phonon emission on a time scale of 1 ps. After that, both lattice and electron gas are at the same temperature. Heat conduction to the surrounding medium then cools the particle back to ambient temperature.

The optical response is governed by the plasmon resonance, itself related to the plasma frequency, ω_p, and the damping time, $\tau = 1/\gamma$. Both quantities are modified by temperature. The damping time decreases with increasing electron gas temperature because more states are accessible by electron−electron scattering.[32] A hot electron gas and a hot lattice both lead to thermal expansion of the particle. This reduces the electron density, which redshifts the plasma frequency and the plasmon resonance with it.[33] Additionally, the retardation effect in Mie's theory depends on the particle size.

Small changes in the plasmon resonance can be detected interferometrically by comparison of the optical properties of the particle before and after heating.[30] A first possibility is to compare two neighbor points in space, as done by differential interference contrast (DIC) microscopy, as in the photothermal method just discussed, and as in the recent pump−probe DIC version of Matsuo and Sasaki.[34] Instead, we propose to interferometrically compare two neighbor points in time. A 1-ps visible (520−650 nm) pulse is split into two orthogonally polarized pulses 10 ps apart after passage through a properly oriented calcite crystal. The first (extraordinary) pulse serves as a reference and the second (ordinary) one as a probe. At a variable delay before or between these two pulses travels the 1-ps infrared (800 nm) pump pulse, which heats the particle. All three pulses are focused on

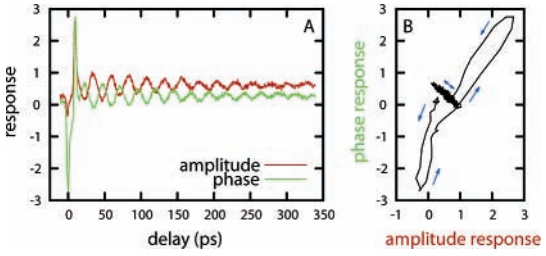

FIGURE 6. Amplitude and phase response (A) of a single 80-nm gold particle to an infrared heating pulse as functions of the delay between the heating and probe pulse. Note that the displayed signal is the difference over the 10-ps time span between the reference and the probe pulse. Panel B shows the same data displayed as a polar plot. Arrows indicate the temporal order. Two separate contributions can be distinguished.

a single gold particle on a cover slide and recollimated by a second objective. The reference and the probe pulses are superimposed in time again by an identical second calcite crystal. A quarter-wave plate and a polarizer allow us to set the working point of the interferometer close to the dark fringe for maximum sensitivity to either amplitude or phase changes. The output of the interferometer is measured using a lock-in amplifier.

Figure 6A shows the time dependence of the amplitude and phase response of a single 80-nm gold particle to the heating pulse. When the amplitude-versus-phase response is plotted (Figure 6B), two different contributions can be distinguished that are rotated by about 90° in the polar plot. The first shorter part is the derivative of a spike-like signal, which can be identified as the increase in plasmon damping during the short period of high electron-gas temperature. The second longer part is a damped oscillation of the amplitude and phase signal around a slowly decreasing average value. This part stems from the breathing mode oscillations of the particle. The steplike increase of the particle size by the heating of the lattice launches elastic oscillations, which are slowly damped.[33] The oscillation period is given by the particle's size and acoustical properties. In an ensemble experiment, particles with different sizes and shapes, placed in different environments, would oscillate at different frequencies. The averaged oscillation would therefore always be damped by inhomogeneous broadening.[35] Because the signal in Figure 6 stems from a single particle, we observe the pure homogeneous damping of the selected nanoparticle in its specific local environment. Because the oscillation period and damping are sensitive to the local environment,[35] a single particle could be used as a mechanical nanosensor. Moreover, our interferometric detection enables us to separate the effect of the real and imaginary parts of the dielectric constant, as done earlier in combined transmission and reflection experiments of metal films.[36−38]

5. Luminescence

Besides scattering of light, metal particles also show photoluminescence under certain conditions. Photoluminescence from metals was first reported by Mooradian[39] in 1969. Local field enhancement at pointed structures increases the emission and modifies the spectra.[40] Especially for very small particles (diameter < 5 nm), the quantum yield increases strongly.[41] Link and El-Sayed have given an overview over radiative properties of gold nanoparticles.[42] We will in the following concentrate on work that has been done on *single* particles.

In 2001, Peyser et al.[43] detected photoactivated luminescence from single silver nanoclusters. An oxidized film of silver islands on a glass cover slide showed individual blinking spots after photoactivation. The spots emitted multicolored luminescence in a dipolar pattern. The emission was attributed to small (2−4 atom) silver clusters on top of silver oxide islands. The clusters change geometry and size under illumination, which leads to dynamic spectral shifts of more than 100 nm. The same group was able to prepare silver clusters of comparable size (2−8 atoms) encaged in a water-soluble dendrimer structure.[44] Five well-separated emission spectra of single clusters could be measured, suggesting that only five different cluster sizes have been created.

Larger structures than the atomic clusters also show blinking luminescence, as demonstrated by Geddes et al.[46] Silver particles of 20−30 nm diameter were prepared by silver nitrate reduction. The emitted intensity shows vivid blinking similar to the above-mentioned clusters, but in this case, multiple emitters per focal volume could not be excluded. Gold particles of slightly larger size (50 nm diameter) were examined by the same group.[47] The blinking behavior is comparable when excited by 532 nm laser light. A detailed discussion of gold nanostructure luminescence was published by Beversluis et al.[45] These authors compare the luminescence of smooth and rough gold films, gold particles, and sharp gold tips. The visible luminescence originates in all cases from the recombination of sp-band electrons with d-band holes. The spectrum is influenced by both the densities of states involved in the transition and the coupling of the recombining pair to far-field radiation.[45] Figure 7a shows the luminescence spectrum of a smooth gold film. The peak around 500 nm is due to an increased density of states for this transition energy, not to a resonance effect. The latter comes into play for 100-nm gold particles. Part b shows the dark-field scattering spectrum of two particles with different plasmon resonances because of asymmetries in the particles. These differences in the plasmon resonance can be found back in their two-photon excited luminescence emission spectrum (part c). The spectra shift together with the plasmon resonance and are blue-shifted with respect to the plasmon spectra because of the increased density of states for short-wavelength transitions, as demonstrated with the smooth gold film in part a.

6. Nonlinear Optical Methods

Besides the pump−probe response, other nonlinear optical effects should be enhanced in the vicinity of metal particles because of the local field enhancement by the plasmon resonance. The nonlinear optical properties of

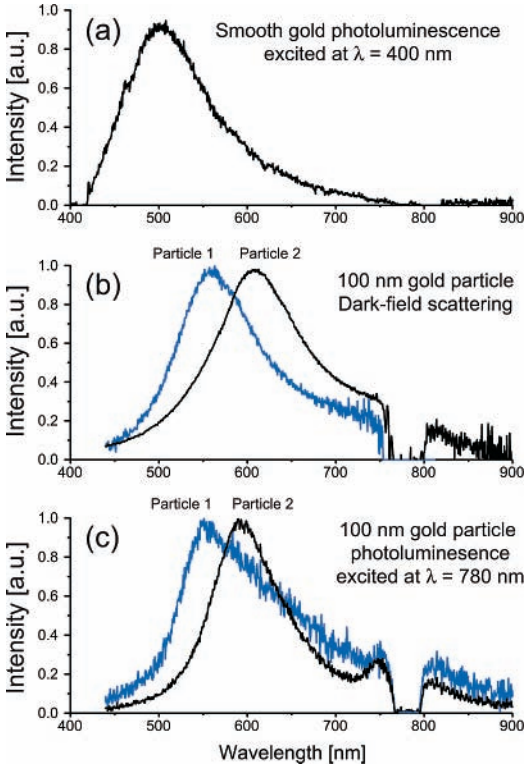

FIGURE 7. One-photon excited luminescence (a) of a smooth gold film, white-light scattering spectra (b) of two 100-nm gold particles, and two-photon excited luminescence spectra (c) of the two particles from panel b. Reprinted with permission from ref 45. Copyright 2003 American Physical Society.

ensembles have been studied in the past,[9] but little work has been done on a single-particle level.

The dephasing time of plasmon oscillations has been measured indirectly in the frequency domain as the homogeneous width of the resonance.[17,22] Liau et al.[48] propose a direct method in the time domain: the measurement of the two-pulse second-order interferometric autocorrelation response. Silver particles of 75 nm diameter were excited with short (23 fs) light pulses at 800 nm. The generation of the second harmonic (SHG) is enhanced because it coincides with the plasmon resonance around 400 nm. The intensity of this SHG signal is measured as function of the delay between two collinear infrared pulses. The first pulse builds up a coherent oscillation of the free metal electrons. If this coherent oscillation is still present when the second pulse arrives, the generation of second harmonic is enhanced. By this method, a dephasing time of 10 fs was measured.[48]

Second-harmonic generation is dipole-forbidden for a perfect spherical particle much smaller than the wavelength. The SHG signal arises from slight deviations from central symmetry and is strongly particle-dependent. Third-harmonic generation (THG), on the other hand, is dipole-allowed. Each particle should produce a signal depending on its size, which would facilitate single-particle labeling and tracking. We thus investigated the THG intensity of single gold particles in the size range of 40−150 nm, accessible to our laser and detection system.[49]

Infrared light pulses (1500 nm, 1 ps) are focused on a single gold particle on a cover slide. The generated light (500 nm) is spectrally filtered and detected by an avalanche photodiode. The THG signal arises from the particle itself and the surrounding medium, for which THG is also dipole-allowed. For a Gaussian beam focused into a homogeneous medium, the Gouy phase shift at the focus leads to exact cancellation of the phase-matched, forward-emitted THG from the bulk medium. However, in our experiment, the particles were lying on a glass−air interface. Contributions from the two sides of the focus no longer cancel, and a strong coherent bulk emission is produced.[50] Because the particle itself is small compared to the beam waist and to the wavelengths, its emission pattern is dipole-like. When recollimated by the high-numerical aperature (NA) objective, the coherent bulk emission is found in the center of the beam, whereas the dipolar particle emission extends over the whole back aperture of the objective.[51] A centered beam-stop therefore suppresses the coherent bulk signal by 5 orders of magnitude, while blocking only 25% of the particle emission.

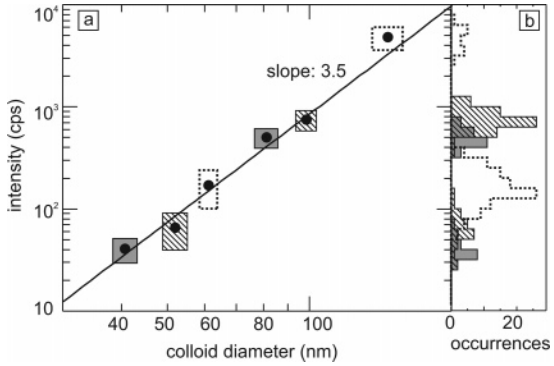

FIGURE 8. Panel a shows average THG intensity (black dots) and width of the intensity distribution (vertical size of the box) of 243 single gold particles in total. The horizontal size of the box gives the size spread of the sample. The data are well-described by a power law with an exponent of 3.5. Panel b shows histograms of THG intensities used to derive the data in panel a.

The individual particles in the size range of 40−150 nm showed a signal stable in time that was proportional to the third power of the excitation intensity and gave a narrow peak in the spectrum at 500 nm. This confirms that we really detect the third-harmonic signal. For a given particle size, the histograms of the peak intensity were monomodal, were clearly separated from the background, and had a relative width coinciding with the size spread of each sample, given by the manufacturer.

Figure 8 shows the size dependence of the THG signal, which varies roughly as the fourth power of diameter. This is compatible with a model by Fomichev et al.[52,53] for the nonlinear excitation of the Mie resonance assuming that the free electrons dominate the nonlinearity. The nonlinear response of *bound* electrons would lead to a sixth-power size dependence.

7. Conclusion

The isolation and study of single gold or silver nanoparticles in the focus of an optical far-field microscope

has recently opened the way to several new experiments and may alter for good the way single biomolecules are tracked and studied. The main advantage of metal probes are their high chemical and physical stability. However, their optical signals are more difficult to extract from background than the luminescence of dye molecules and semiconductor nanocrystals. Several methods have been proposed to detect, identify, image, and analyze noble-metal particles as small as a few nanometers in diameter with a high signal-to-noise ratio and a good selectivity against other scattering or absorbing structures. Direct observation of scattering is straightforward and gives access to sizes as small as 5−10 nm in perfect conditions (e.g., particles dispersed at a glass−air interface). It is limited to rather large sizes if the particles are in a turbid or scattering environment such as a cell. To discriminate a metal particle against its nonmetallic surroundings, one can exploit specific properties, such as the absorption of energy and subsequent medium heating by the particle or the transient changes of optical response following absorption of a short laser pulse. In the latter case, different delay times relate to different contrast mechanisms, from some tens of femtoseconds for electron−electron thermalization to picoseconds for electron−lattice interaction and tens of picoseconds for lattice cooling and elastic oscillations. Other nonlinear optical signals such as second- or third-harmonic generation can also provide optical contrast for metal particles and be used in combination with nonlinear microscopy of biological samples. While the detection of noble-metal particles is greatly facilitated by their intense plasmon resonance, the current optical techniques are already sensitive enough to detect single particles of other metals, opening a broad range of new effects (e.g., nanomechanics, magnetism, etc.) to far-field optical investigation. We expect new applications of metal labels to multiply in the next few years, opening a wealth of new possibilities for biological and material sciences.

M.L. acknowledges a Marie Curie Fellowship from the European Commission (Contract No. HPMF-CT-2002-02099). This work is part of the research program of the "Stichting voor Fundamenteel Onderzoek der Materie" (FOM), financially supported by the NWO.

References

(1) Special issue on Single Molecules. *Science* **1999**, *283*, 1593−1804.
(2) Tamarat, P.; Maali, A.; Lounis, B.; Orrit, M. Ten years of single-molecule spectroscopy. *J. Phys. Chem. A* **2000**, *104*, 1−16.
(3) Michalet, X.; Pinaud, F.; Lacoste, T. D.; Dahan, M.; Bruchez, M. P.; Alivisatos, A. P.; Weiss, S. Properties of fluorescent semiconductor nanocrystals and their application to biological labeling. *Single Mol.* **2001**, *2*, 261−276.
(4) Hillenbrand, R.; Keilmann, F. Optical oscillation modes of plasmon particles observed in direct space by phase-contrast near-field microscopy. *Appl. Phys. B* **2001**, *73*, 239−243.
(5) Klar, T.; Perner, M.; Grosse, S.; von Plessen, G.; Spirkl, W.; Feldmann, J. Surface-plasmon resonances in single metallic nanoparticles. *Phys. Rev. Lett.* **1998**, *80*, 4249−4252.
(6) Wiederrecht, G. P. Near-field optical imaging of noble metal nanoparticles. *Eur. Phys. J.: Appl. Phys.* **2004**, *28*, 3−18.
(7) Kneipp, K.; Kneipp, H.; Itzkan, I.; Dasari, R. R.; Feld, M. S. Surface-enhanced Raman scattering and biophysics. *J. Phys.: Condes. Matter* **2002**, *14*, R597−624.
(8) Johnson, P. B.; Christy, R. W. Optical-Constants Of Noble-Metals. *Phys. Rev. B* **1972**, *6*, 4370−4379.
(9) Kreibig, U.; Vollmer, M. *Optical Properties of Metal Clusters*; Springer Series in Materials Science, Vol. 25; Springer: Berlin, 1995.
(10) Bohren, C. F.; Huffman, D. R. *Absorption and Scattering of Light by Small Particles*; Wiley: New York, 1998.
(11) van de Hulst, H. C. *Light Scattering by Small Particles*; Dover Publications: New York, 1981.
(12) Raether, H. *Surface Plasmons*; Springer Tracts in Modern Physics, Vol. 111; Springer: Berlin, 1988.
(13) Raschke, G.; Kowarik, S.; Franzl, T.; Sönnichsen, C.; Klar, T. A.; Feldmann, J.; Nichtl, A.; Kurzinger, K. Biomolecular recognition based on single gold nanoparticle light scattering. *Nano Lett.* **2003**, *3*, 935−938.
(14) McFarland, A. D.; Van Duyne, R. P. Single silver nanoparticles as real-time optical sensors with zeptomole sensitivity. *Nano Lett.* **2003**, *3*, 1057−1062.
(15) Schultz, S.; Smith, D. R.; Mock, J. J.; Schultz, D. A. Single-target molecule detection with nonbleaching multicolor optical immunolabels. *Proc. Natl. Acad. Sci. U.S.A.* **2000**, *97*, 996−1001.
(16) Sönnichsen, C.; Franzl, T.; Wilk, T.; von Plessen, G.; Feldmann, J. Plasmon resonances in large noble-metal clusters. *New J. Phys.* **2002**, *4*, 93.1−93.8.
(17) Sönnichsen, C.; Franzl, T.; Wilk, T.; von Plessen, G.; Feldmann, J.; Wilson, O.; Mulvaney, P. Drastic reduction of plasmon damping in gold nanorods. *Phys. Rev. Lett.* **2002**, *88*, No. 077402.
(18) Rechberger, W.; Hohenau, A.; Leitner, A.; Krenn, J. R.; Lamprecht, B.; Aussenegg, F. R. Optical properties of two interacting gold nanoparticles. *Opt. Commun.* **2003**, *220*, 137−141.
(19) Haes, A. J.; Van Duyne, R. P. A unified view of propagating and localized surface plasmon resonance biosensors. *Anal. Bioanal. Chem.* **2004**, *379*, 920−930.
(20) Schultz, D. A. Plasmon resonant particles for biological detection. *Curr. Opin. Biotechnol.* **2003**, *14*, 13−22.
(21) Itoh, T.; Asahi, T.; Masuhara, H. Femtosecond light scattering spectroscopy of single gold nanoparticles. *Appl. Phys. Lett.* **2001**, *79*, 1667−1669.
(22) Sönnichsen, C.; Geier, S.; Hecker, N. E.; von Plessen, G.; Feldmann, J.; Ditlbacher, H.; Lamprecht, B.; Krenn, J. R.; Aussenegg, F. R.; Chan, V. Z. H.; Spatz, J. P.; Moller, M. Spectroscopy of single metallic nanoparticles using total internal reflection microscopy. *Appl. Phys. Lett.* **2000**, *77*, 2949−2951.
(23) Nakayama, H.; Yamaga, T.; Kunioka, Y. Fine profile of actomyosin motility fluctuation revealed by using 40-nm probe beads. *Biochem. Biophys. Res. Commun.* **1998**, *246*, 261−266.
(24) Lindfors, K.; Kalkbrenner, T.; Stoller, P.; Sandoghdar, V. Detection and spectroscopy of gold nanoparticles using supercontinuum white light confocal microscopy. *Phys. Rev. Lett.* **2004**, *93*, No. 037401.
(25) Debrabander, M.; Nuydens, R.; Geuens, G.; Moeremans, M.; Demey, J. Microtubule Dependent Motility Investigated With Nanometer Particle Video Microscopy (Nanovid). *Cell Motil. Cytoskeleton* **1986**, *6*, 238−238.
(26) Arbouet, A.; Christofilos, D.; Del Fatti, N.; Vallée, F.; Huntzinger, J. R.; Arnaud, L.; Billaud, P.; Broyer, M. Direct measurement of the single-metal-cluster optical absorption. *Phys. Rev. Lett.* **2004**, *93*, No. 127401.
(27) Boyer, D.; Tamarat, P.; Maali, A.; Lounis, B.; Orrit, M. Photothermal imaging of nanometer-sized metal particles among scatterers. *Science* **2002**, *297*, 1160−1163.
(28) Cognet, L.; Tardin, C.; Boyer, D.; Choquet, D.; Tamarat, P.; Lounis, B. Single metallic nanoparticle imaging for protein detection in cells. *Proc. Natl. Acad. Sci. U.S.A.* **2003**, *100*, 11350−11355.
(29) Berciaud, S.; Cognet, L.; Blab, G. A.; Lounis, B. Photothermal Heterodyne Imaging of Individual Nonfluorescent Nanoclusters and Nanocrystals. *Phys. Rev. Lett.* **2004**, *93*, No. 257402.
(30) van Dijk, M. A.; Lippitz, M.; Orrit, M. Interferometric pump−probe spectroscopy of single gold colloids. Manuscript in preparation.
(31) Voisin, C.; Del Fatti, N.; Christofilos, D.; Vallée, F. Ultrafast electron dynamics and optical nonlinearities in metal nanoparticles. *J. Phys. Chem. B* **2001**, *105*, 2264−2280.
(32) Perner, M.; Bost, P.; Lemmer, U.; von Plessen, G.; Feldmann, J.; Becker, U.; Mennig, M.; Schmitt, M.; Schmidt, H. Optically induced damping of the surface plasmon resonance in gold colloids. *Phys. Rev. Lett.* **1997**, *78*, 2192−2195.
(33) Hartland, G. V. Coherent vibrational motion in metal particles: Determination of the vibrational amplitude and excitation mechanism. *J. Chem. Phys.* **2002**, *116*, 8048−8055.
(34) Matsuo, Y.; Sasaki, K. Time-resolved laser scattering spectroscopy of a single metallic nanoparticle. *Jpn. J. Appl. Phys., Part 1* **2001**, *40*, 6143−6147.
(35) Voisin, C.; Christofilos, D.; Del Fatti, N.; Vallée, F. Environment effect on the acoustic vibration of metal nanoparticles. *Physica B* **2002**, *316*, 89−94.

(36) Del Fatti, N.; Voisin, C.; Christofilos, D.; Vallée, F.; Flytzanis, C. Acoustic vibration of metal films and nanoparticles. *J. Phys. Chem. A* **2000**, *104*, 4321−4326.
(37) Perrin, B.; Rossignol, C.; Bonello, B.; Jeannet, J. C. Interferometric detection in picosecond ultrasonics. *Physica B* **1999**, *263*, 571−573.
(38) Kop, R. H. J.; deVries, P.; Sprik, R.; Lagendijk, A. Kramers−Kronig relations for an interferometer. *Opt. Commun.* **1997**, *138*, 118−126.
(39) Mooradian, A. Photoluminescence Of Metals. *Phys. Rev. Lett.* **1969**, *22*, 185−187.
(40) Boyd, G. T.; Yu, Z. H.; Shen, Y. R. Photoinduced Luminescence From The Noble-Metals And Its Enhancement On Roughened Surfaces. *Phys. Rev. B* **1986**, *33*, 7923−7936.
(41) Wilcoxon, J. P.; Martin, J. E.; Parsapour, F.; Wiedenman, B.; Kelley, D. F. Photoluminescence from nanosize gold clusters. *J. Chem. Phys.* **1998**, *108*, 9137−9143.
(42) Link, S.; El-Sayed, M. A. Shape and size dependence of radiative, nonradiative and photothermal properties of gold nanocrystals. *Int. Rev. Phys. Chem.* **2000**, *19*, 409−453.
(43) Peyser, L. A.; Vinson, A. E.; Bartko, A. P.; Dickson, R. M. Photoactivated fluorescence from individual silver nanoclusters. *Science* **2001**, *291*, 103−106.
(44) Zheng, J.; Dickson, R. M. Individual water-soluble dendrimer-encapsulated silver nanodot fluorescence. *J. Am. Chem. Soc.* **2002**, *124*, 13982−13983.
(45) Beversluis, M. R.; Bouhelier, A.; Novotny, L. Continuum generation from single gold nanostructures through near-field mediated intraband transitions. *Phys. Rev. B* **2003**, *68*, No. 115433.
(46) Geddes, C. D.; Parfenov, A.; Gryczynski, I.; Lakowicz, J. R. Luminescent blinking of gold nanoparticles. *Chem. Phys. Lett.* **2003**, *380*, 269−272.
(47) Geddes, C. D.; Parfenov, A.; Gryczynski, I.; Lakowicz, J. R. Luminescent blinking from silver nanostructures. *J. Phys. Chem. B* **2003**, *107*, 9989−9993.
(48) Liau, Y. H.; Unterreiner, A. N.; Chang, Q.; Scherer, N. F. Ultrafast dephasing of single nanoparticles studied by two-pulse second-order interferometry. *J. Phys. Chem. B* **2001**, *105*, 2135−2142.
(49) Lippitz, M.; van Dijk, M. A.; Orrit, M. Third-Harmonic Generation from Single Gold Nanoparticles. *Nano Lett.* ASAP, DOI 10.1021/nl0502571.
(50) Schins, J. M.; Schrama, T.; Squier, J.; Brakenhoff, G. J.; Mü×b9ller, M. Determination of material properties by use of third-harmonic generation microscopy. *J. Opt. Soc. Am. B* **2002**, *19*, 1627−1634.
(51) Courtois, J. Y.; Courty, J. M.; Mertz, J. C. Internal dynamics of multilevel atoms near a vacuum-dielectric interface. *Phys. Rev. A* **1996**, *53*, 1862−1878.
(52) Fomichev, S. V.; Popruzhenko, S. V.; Zaretsky, D. F.; Becker, W. Laser-induced nonlinear excitation of collective electron motion in a cluster. *J. Phys. B* **2003**, *36*, 3817−3834.
(53) Fomichev, S. V.; Popruzhenko, S. V.; Zaretsky, D. F.; Becker, W. Nonlinear excitation of the Mie resonance in a laser-irradiated cluster. *Opt. Express* **2003**, *11*, 2433−2439.

AR0401303